FULL PAPER

Precise tilt measurement by seafloor borehole tiltmeters at the Nankai Trough subduction zone

Shuhei Tsuji[1]*, Eiichiro Araki[1], Takashi Yokobiki[1], Shuhei Nishida[1], Yuya Machida[1], Mark Zumberge[2] and Keisuke Takahashi[3]

Abstract

In this study, geodetic and seismic phenomena occurring in the subduction zone were observed with two tiltmeters that were installed in seafloor boreholes drilled in the Kumano Basin in the Nankai Trough, southwest Japan. We used one electrolytic-type tiltmeter and one pendulum-type tiltmeter installed 6 and 19 m below the seafloor, respectively. The two tiltmeters have been continuously operated since 2019 and 2021, respectively. The records of the two tiltmeters showed microseisms, seismic signals of normal earthquakes, and variations that correlated well with the M2 tide (tidal response). The noise environment relative to existing seafloor observatories was assessed by comparing the power spectral densities of the tiltmeters and broadband seismometers in the seismic frequency band. The two tiltmeters and the seismometers showed similar spectral peaks in the microseism band, and at lower frequencies below 10^{-2} Hz, the pendulum tiltmeter had a noise level that was up to 20 dB lower than that of the broadband seismometers. The tidal responses of the tiltmeters were analyzed to reveal corresponding mechanisms because a large amplitude of the tidal response makes it difficult to detect geodetic phenomena. Considerable azimuthal dependence was observed in the NW–SE direction for both tiltmeters. The principal direction was approximately the same as the down-slope direction of the local bathymetry. This tendency was thus interpreted to be caused by the differences in the thickness of the sedimentary layer along the direction of the slope. Furthermore, the validity of the tilt measurements for the two tiltmeters was demonstrated by in-situ loading experiments, where the theoretical response of an elastic half-space medium was computed and compared with the experimental results. The results of the loading experiments can be explained using theoretical values with a set of realistic elastic moduli.

Keywords Tilt, Seafloor borehole, Nankai trough, Optical sensing, Tide, Long-term observation, Azimuthal dependence, Tidal response
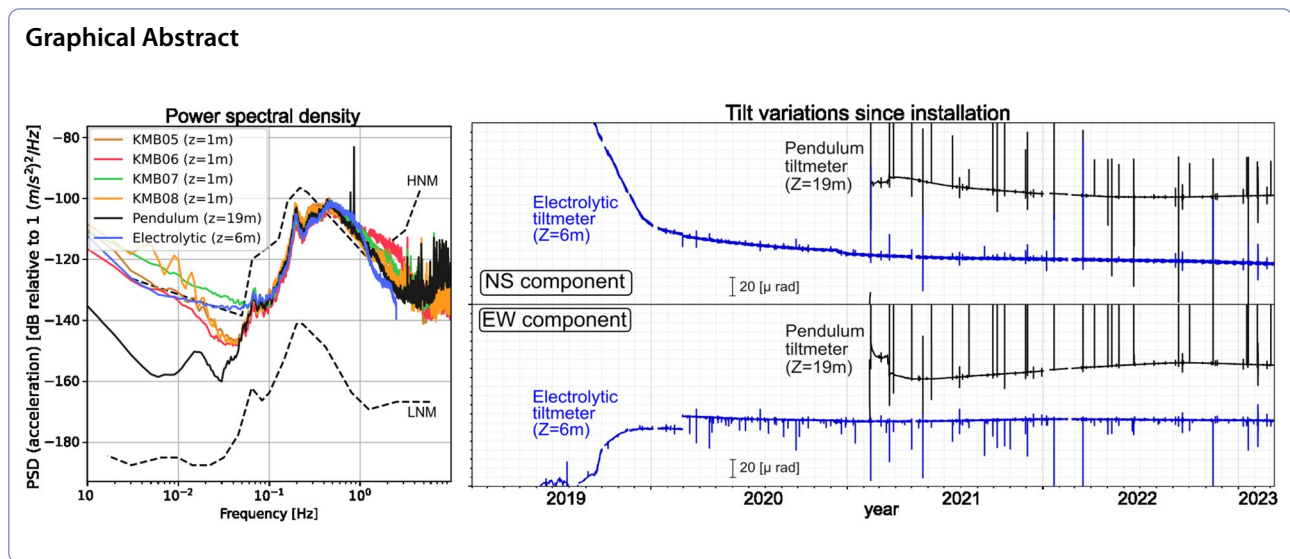
---

*Correspondence:
Shuhei Tsuji
stsuji@jamstec.go.jp
Full list of author information is available at the end of the article

Graphical Abstract

Introduction

The Nankai Trough is one of the most famous subduction zones. The Philippine Sea Plate is subducting beneath the Amour Plate in the NE-SW direction at a rate of 6 cm/year (Argus et al. 2011). This subduction process causes M8-class earthquakes at intervals of 100–200 years (e.g., Ando 1975), several large (> Mw 7) earthquakes such as the 2004 off the Kii peninsula earthquake (Japan Meteorological Agency 2004), and several slow earthquakes (Nakano et al. 2018; Takemura et al. 2022; Yamamoto et al. 2022).

The observation network in the Nankai Trough region is expanding toward the sea to closely observe phenomena associated with subduction processes. The "Dense Ocean Floor Network System for Earthquakes and Tsunamis" (DONET) was developed in the Kumano Basin off the Kii Peninsula for continuous seismic observations (National Research Institute for Earth Science and Disaster Resilience 2019; Kawaguchi et al. 2011, 2015; Kaneda et al. 2015). As broadband seismometers were deployed at DONET stations, the observations contributed to recent studies on slow earthquakes (Annoura et al. 2017; Nakano et al. 2018; Toh et al. 2020; Yamamoto et al. 2022). Measurements of seafloor displacement using the GNSS-A technique have been repeatedly performed, which revealed coseismic deformation of the seafloor after the 2004 earthquake (Kido et al. 2006) and improved the accuracy of the coupling rate on the plate surface (Yokota et al. 2016; Nishimura et al. 2018).

DONET plays an important role in the continuous observation of sea areas. Compared to studies with ocean bottom seismometers (Obana and Kodaira 2009; Tamaribuchi et al. 2019), continuous observations with buried permanent seismometers at DONET stations enable integration of temporal resolution and detectability. Furthermore, DONET provides electrical power and communication between the land stations and seafloor, which can be used for several observations. For example, a package of seismic and geodetic sensors called the "Long-Term Borehole Monitoring System (LTBMS)" was installed in three boreholes drilled in the Integrated Ocean Drilling Program (IODP) using the deep-sea scientific drilling vessel Chikyu and connected to DONET. Pore pressure measurements by the LTBMS stations revealed variations in slow-slip events and those associated with shallow very low frequency earthquakes (VLFEs) (Araki et al. 2017; Ariyoshi et al. 2021).

In this study, two different types of tiltmeters were installed in the Kumano Basin at different seafloor borehole depths (Figs. 1 and 2) to detect seismic and geodetic phenomena, such as VLFEs and short-term slow slip events (SSEs), with better resolution than that achieved in previous observations. One tiltmeter was a high-precision electrolytic-type tiltmeter that was installed in an 8.6 m-deep borehole in 2019. The other tiltmeter was a pendulum tiltmeter that was based on an optical geodetic sensor (Zumberge et al. 2018) and installed in a 20 m-deep borehole in 2021 (Yokibiki et al. 2023). This study reports the characteristics of the first three and two years of the tilt records, respectively, and discusses the detectability and validity of tilt observations through power spectral density (PSD) analysis and in-situ load experiments.

Measurement system

The objective was to develop methods of installation and measurement using a low-noise environment of the borehole within a reachable depth by considering the wide
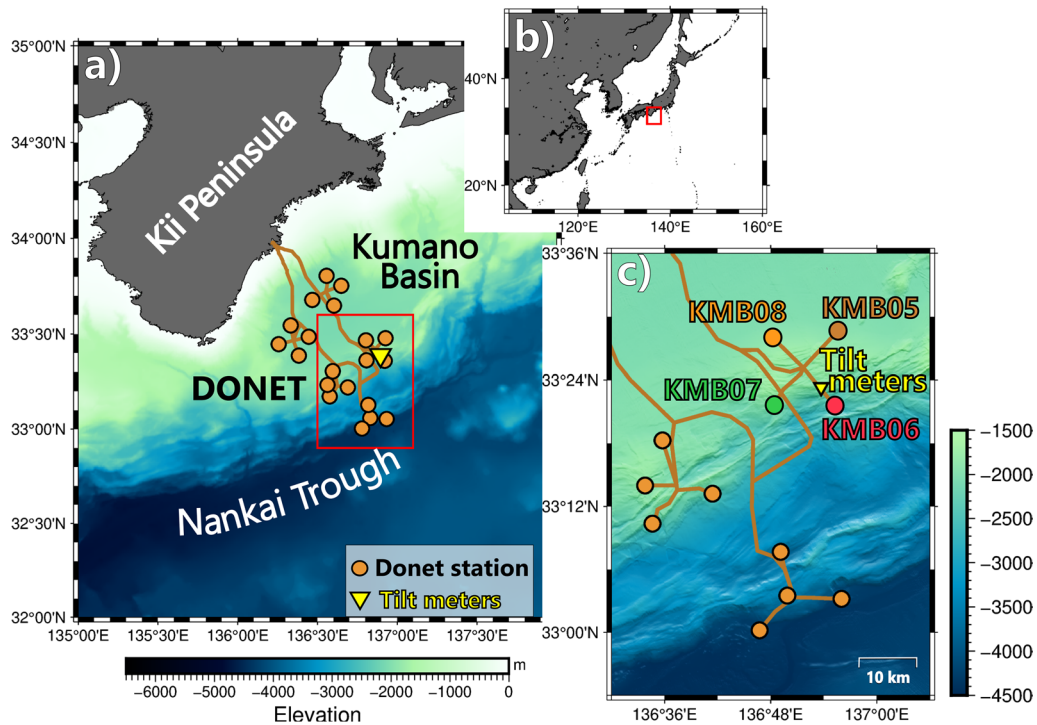
Tsuji *et al. Earth, Planets and Space* (2023) 75:188

Page 3 of 14

Fig. 1 Map of the study area. The locations of the tiltmeters and DONET stations are shown. Red squares in **a** and **b** indicate areas of the maps **c** and **b**, respectively. The color of the markers for KMB05 to KMB07 corresponds to the color of lines in Fig. 6
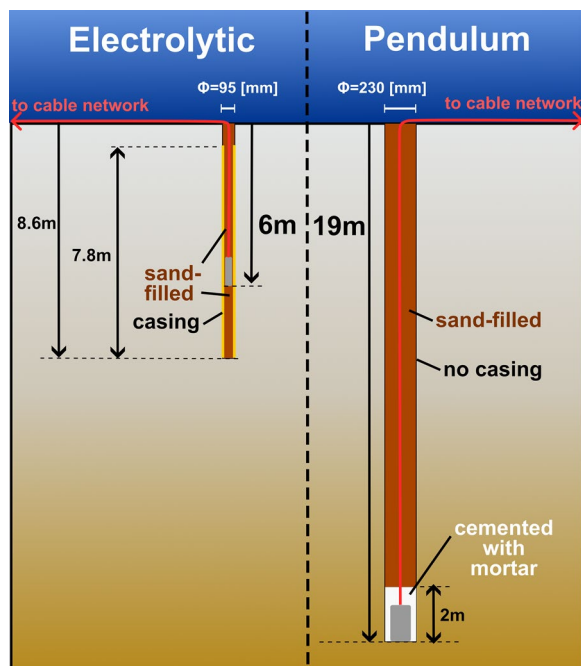

Fig. 2 Depth and installation conditions for the two tiltmeters. Schematic illustration of tiltmeters in boreholes. The electrolytic tiltmeter was installed 6 m below the seafloor and surrounded by sand. The pendulum tiltmeter was installed 19 m below the seafloor and cemented with mortar to couple the tiltmeter with the surrounding media

expansion of the observation network. Burying a sensor is an effective way to reduce noise levels. For example, Araki et al. (2013) reported an 80 dB reduction in the noise level in a seismic band by burying a sensor 1 m below the seafloor. However, deep boreholes deeper than several hundreds of meters, such as those drilled by the IODP, are expensive. Therefore, in the first station of this study, a borehole was drilled to a depth of 8.6 m below the seafloor, and a tiltmeter was installed at a depth of 6 m. Based on the experiences of the first station, for the second station, a 20 m-deep borehole was drilled 80 m away from the first station. Additionally, to fully utilize the low-noise environment, a tiltmeter more sensitive than the first one was developed and used in the second station.

In the development of the first station, an electrolytic tiltmeter, the "Lily self-leveling borehole tiltmeter" made by Jewell Instruments (formally Applied Geometrics Inc.), was selected as the tilt sensor. The Lily has a resolution of less than 5 nrad for the tilt measurement and a 10° of self-leveling range. This tiltmeter was used for tilt measurements in the LTBMS of the IODP. Its performance was assessed as described by Kimura et al. (2013). In their work, a power spectral density analysis was conducted to assess the availability of installation in a borehole.

Tsuji *et al. Earth, Planets and Space*   (2023) 75:188

Page 4 of 14

An 8.6 m-deep borehole was drilled using a boring machine system (BMS), and a tiltmeter was installed in the borehole at a depth of 6 m. Figure 2 presents an overview of the tiltmeter installation conditions. The borehole was drilled to 8.6 m below the seafloor by the BMS during the KM18-09 cruise of the R/V Kaimei. A 7.8 m long casing was used during drilling, and was left in the borehole. The tiltmeter was inserted into the casing and stacked at a depth of 6 m due to friction between cables and the casing. The borehole was subsequently filled with sand so that the tiltmeter was surrounded by sand to a depth of 6 m of the 8.6 m-deep borehole.

The tiltmeter was connected to the DONET on the seafloor through an interface unit using an optical fiber network for electrical power supply and communication. This mechanism made long-term and stable observations possible. The data measured by the tiltmeter were transferred to a land station in real time via DONET. Then, the data were acquired at the land station and were synchronized with the data center to monitor real-time measurements.

During the development of the second station, a specific tiltmeter, which was developed based on an optical geodetic sensor (Zumberge et al. 2018), was used to measure the precise tilt variation in a broader frequency band. The tiltmeter was capable of measuring tilt variation in two horizontal components by measuring the displacement of the mass of two pendulums installed perpendicularly. Mass displacements were measured using a Michelson interferometer, which is an optical ranging technique that enables the detection of small changes in length. The theoretical sensitivities in the tilt measurements calculated from the optical measurement conditions were 3.421×10^{-4} and 2.753×10^{-4} nrad for the X and Y components, respectively. No feedback during the measurement is another advantage of this device. The sensor's 40 cm pendulums can swing through a very large dynamic range of ± 3 degrees, allowing "self leveling" without the need for motorized actuators, as in the case of the Lily tiltmeter. The sensor is simplified by not needing feedback, and its dynamic range equivalent to 32 bits would not be practical using electronics. This mechanism enables precise measurement of the tilt, especially for long-term phenomena. The mass displacements were computed using a microprocessor built on the tiltmeter using the algorithm developed by Zumberge et al. (2004). Using this specific algorithm, mass displacements were obtained at 200 Hz sampling. Therefore, the tiltmeter can be used as an acceleration-type seismometer. The results were compiled into "win format" data (Urabe and Tsukada 1992) and transferred to the land station via DONET. Additionally, DONET provided the time information

obtained by the clock of the global positioning system (GPS) to the tiltmeter. Using the time information, the error of the internal clock was precisely calculated and attached to the tilt records. Thus, the accuracy of the time was in the order of microseconds.

The performance of the pendulum tiltmeter was assessed via on-land tests at the Kamioka mine, which is located in at the central part of Honshu Island, Japan (Kimura et al. 2021). Analysis of power spectral density and phase using ambient noise and teleseismic records confirmed the validity of the pendulum tiltmeter from approximately 0.001 Hz to several Hz. In addition, same level of stability was confirmed by comparison of the tilt record with the electrolytic tiltmeter.

Since the tiltmeter used pendulums, the displacement of the pendulum was converted to the ground tilt. First, the mass displacement was converted to ground acceleration based on Zumberge et al. (2018). Then, the ground acceleration was converted to ground tilt, assuming that the variations in acceleration were due to variations in the tilt. We used Eq. (1) to obtain the ground acceleration $\ddot{z}$:

$$\ddot{x} + \frac{\omega_0}{Q}\dot{x} + \omega_0^2 x = -G\ddot{z} \tag{1}$$

where x is the mass displacement, ω_0 is the natural frequency of a pendulum, Q is the damping factor of the pendulum, and G is a constant that depends on mechanical settings and flexure stiffness. First and second time derivatives are indicated by dot notation. Then, tilt θ was calculated by $\theta = -\sin^{-1}(\ddot{z}/g)$, in which g is the gravitational acceleration. Since the parameters ω_0 and Q change slightly with the environment, they were estimated with the spectral shape on each day. The parameters were estimated by fitting the ensemble spectra of the mass movement around the natural frequency of the pendulums to the amplitude of the transfer function of the instrumental response. This is because the shape of the transfer function spectrum changes depending on the parameters. The ensemble spectra were calculated within a 15 min trace without earthquake signals in a day.

The installation process of the pendulum tiltmeter was modified from a previous electrolytic tiltmeter. The details of the process have been reported by Yokibiki et al. (2023). To reduce the environmental noise to below that of the first station, a borehole was drilled down to 19 m below the seafloor using the BMS. Drilling was performed during the KM21-E01 cruise of the R/V Kaimei. Furthermore, mortar was used to couple the tiltmeter to the surrounding media. The tiltmeter was cemented at 19 m below the surface onto a 2 m mortar layer (Fig. 2). The upper part of the mortar layer was filled with sand.

Tsuji *et al. Earth, Planets and Space*   (2023) 75:188

Page 5 of 14

Observations

The tilt variations in the first three and two years are shown in Fig. 3. Large initial drifts were observed for both tiltmeters. Furthermore, the duration and magnitude of the initial drifts for the two sensors differed. The electrolytic tiltmeter exhibited a larger drift over a longer period, with the magnitude of the initial drift exceeding 100 μrad, which continued for approximately two years. On the contrary, for the pendulum tiltmeter, the initial drift was less than 50 μrad in magnitude and continued for approximately 1.5 years. This difference could have been caused by differences in installation methods. As expected from the system development, the method using mortar, quickly and effectively coupled the sensor with the surrounding media.

Next, the orientations of the sensors were estimated by comparing the earthquake signals with those of the nearest broadband seismometers in DONET. The method used by Nakano et al. (2012), which is a study to estimate the sensor orientations of the DONET stations, was used to estimate the orientations of the tiltmeter sensors. This method searches for the rotation angle with the maximum correlation of long-period seismic waveforms. Because the orientations of DONET stations have already been estimated by Nakano et al. (2012), the correlation of seismic records observed by tiltmeters was calculated with respect to those observed by the four DONET stations in the nearest node (KMB05, KMB06, KMB07, and KMB08). The correlation was calculated at intervals of one degree to find the orientation with the maximum correlation. In this calculation, the velocity waveforms observed by the DONET stations were converted into acceleration waveforms for phase comparison with the tiltmeters. A band-pass filter between 100 and 125 s was applied to the seismic records.

Consequently, $N170°E \pm 8.5°$ and $N190°E \pm 11°$ were estimated for the orientation of the Y direction in the right-handed Cartesian coordinate system of the pendulum and electrolytic tiltmeter, respectively. Seven regional deep earthquakes of M 4.2 to M 6.0 were used for the estimation. As four DONET stations were used for the estimation, 28 sets of waveforms were obtained. Orientations of the tiltmeters are estimated with each waveform by calculation of the maximum correlations. Among them, 19 and six sets of results were selected based on a correlation coefficient threshold of 0.95 for the pendulum and electrolytic tiltmeter, respectively. Results with a low correlation coefficient were mainly due to the step of the pendulum tiltmeter or distortion of the waveform due to an offset of the sensor of the electrolytic tiltmeter from the self-leveling position at initial conditions. The selected results were then averaged to estimate the orientation.

In the tilt record of the pendulum tiltmeter, step-like changes were frequently and continuously observed (Figs. 4a, b). Such changes were observed only in the tilt record of the pendulum tiltmeter, although the electrolytic tiltmeter was installed only 80 m away. A total of 762 steps were observed after 750 days of analysis. In most cases, the duration of the step-like changes was less than 20 min. The minimum and maximum magnitude of the steps, which is the square root of the sums of squares of
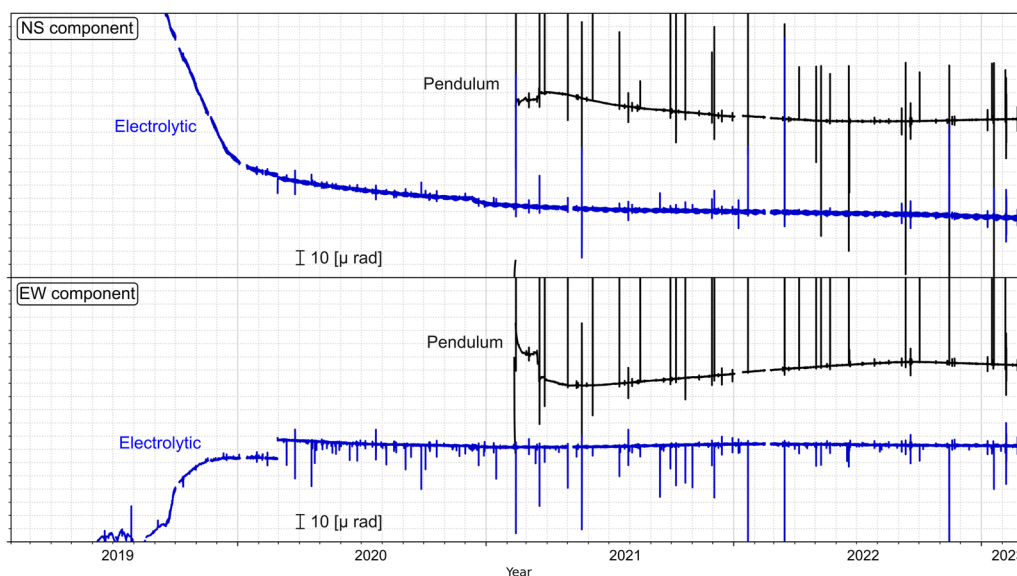

Fig. 3 Tilt variations in the two tiltmeters since installation. The blue and black lines show the electrolytic and pendulum tiltmeters, respectively. Gaps in the data indicate the lack of data due to troubles with the data acquisition system. Vertical spikes in tilt variations show earthquake signals
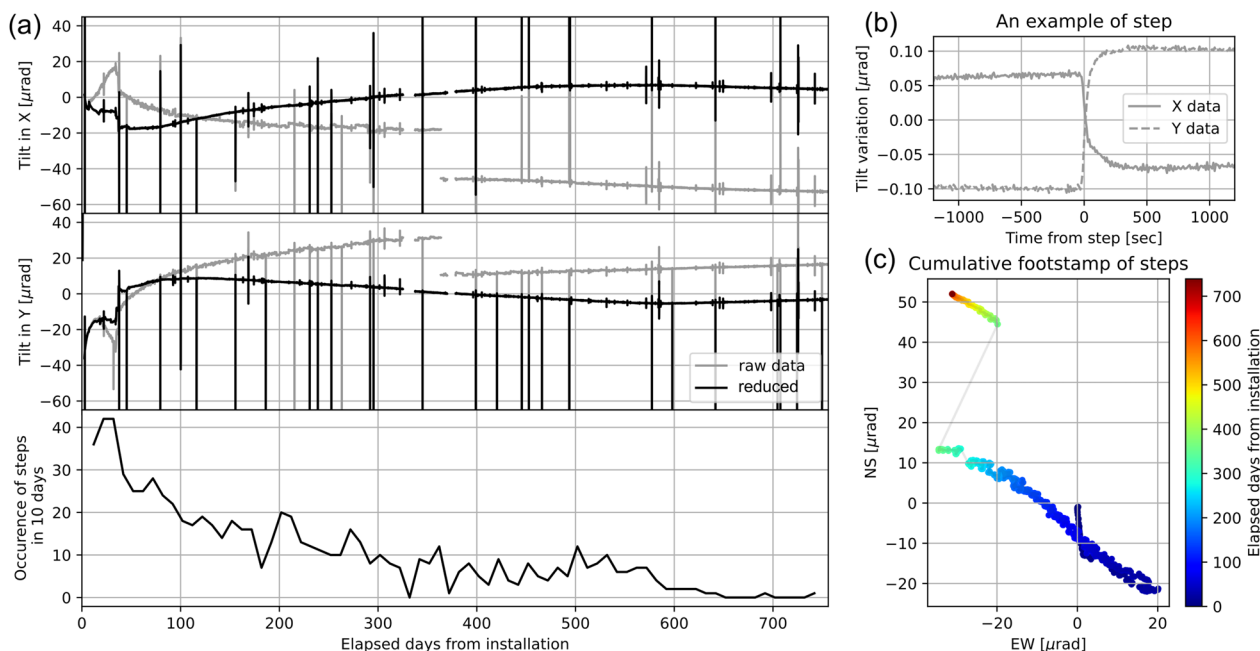
Tsuji *et al. Earth, Planets and Space*   (2023) 75:188

Page 6 of 14

Fig. 4 Characteristics of the steps **a** Raw and reduced tilt variation and occurrence frequency of steps in 10 days; **b** An example of a step in a time series; and **c** cumulative amount of steps in the horizontal plane. In the top two panels in (**a**), gray and black lines show the raw tilt variation and tilt variation after reduction of the step. In (**a**) and (**b**), X and Y components indicate each component of the sensor of the pendulum tiltmeter. In (**c**), the color of each data point indicates the elapsed time since installation

the step amplitude in the X and Y directions of the sensor, were 4.5 nano radians and 34 micro radians, respectively. The largest step occurred on February 9, 2022, and had an exceptionally large amplitude. Except of this step, the maximum magnitude is 4.4 micro radians, and the average and standard deviation of the steps were 0.38 and 0.50 micro radians, respectively. Additionally, the frequency of occurrence decreased over time.

To analyze the mechanism of the step-like changes, the cumulative movement due to the steps over time and their azimuthal dependency were analyzed. The NW–SE direction was the predominant step direction, except immediately after installation and the large step on February 9, 2022 (Fig. 4c). Based on these characteristics, the mechanism of the step was interpreted as the movement to a stable position in small displacements. Since the height of the pressure vessel that contained the pendulum tiltmeter was 1.3 m, one microradian of tilt was equal to less than 1.3×10^{-6} m of displacement, which is the realistic size of a small pore created by hydraulic confinement on porous media. It has been reported that when hydraulic pressure acts on a porous material such as cement mortar for a long period, changes in volumetric strain ranging from tens of μ to hundreds of μ occur intermittently (Takahashi et al. 2022). Moreover, a reduction in the frequency of occurrence suggests that the tiltmeter is approaching a stable position. However, the

existence of a predominant direction is inconsistent with the results reported by Takahashi et al. (2022).

This azimuthal dependency may reflect weakness of the sediments around the borehole. Theoretically, the pore structure of mortar forms isotopically in a given space. However, if the strength of the sediments is anisotropic, anisotropy occurs in the creation of pore structure and the larger response would be observed in the softer or weaker direction of the surrounding sediments. An offset of the center of the tiltmeter and the borehole can result in azimuthal dependency. If the offset is a cause of the azimuthal dependency, the offset should be large to obtain a significant small variation in cumulative movement in the perpendicular direction to the dominant direction in Fig. 4c. However, it is inconsistent with the fact that the tiltmeter was fixed approximately at the center by a centralizer. Thus, the offset of the centers would not be the cause.

As the steps are thought to be related to the installation process, they were reduced under the assumption that no tilt change occurred immediately before or after a step. The step magnitude was calculated as the difference between the averages of the tilt records in a constant time window before and after the step. Using this magnitude, the tilt records after the step were adjusted to the same level as those before the step. The tilt records during each step were interpolated using the average tilt in the time

Tsuji *et al. Earth, Planets and Space*   (2023) 75:188

Page 7 of 14

window prior to the step. Of the 762 steps, 713 had a duration shorter than 20 min, and the other 49 steps had longer durations. Thus, 20 and 40 min were used as the lengths of the time window for the normal and longer steps, respectively.

In the stable period after the initial drift, a large magnitude of tilt variation with a duration of approximately 12 h was observed for both tiltmeters. The tilt variation correlated well with the pressure change observed by the seafloor pressure meter at the nearest DONET station (Fig. 5a), although only the horizontal components were measured. The predominant period of the change was the M2 tide. Hereinafter, this tilt variation is termed the "tidal response". The amplitude of the electrolytic tiltmeter was approximately ten times larger than that of the pendulum tiltmeter. The amplitude of the NS component was greater than that of the EW component, particularly for the electrolytic tiltmeter. This tendency and their azimuthal dependency are discussed in the "Discussion" section.

Discussions
Noise level and detectability of VLFEs
To assess the noise environment of the obtained observations, the ensemble power spectral density (PSD) of the tiltmeters was compared with those of four broadband seismometers in DONET (KMB04, KMB05, KMB06 and KMB07) around the tiltmeters. To compare the PSD between the tiltmeters and seismometers, we converted

their record to acceleration records. In this calculation, tilt is converted to acceleration by $\ddot{z} = -g\theta$, where $\ddot{z}$ is the acceleration, g is the gravity acceleration, and θ is the tilt. The natural frequency of the seismometers at DONET stations was 360 s. The PSD was calculated for each day in November 2022, when the number of the step-like changes of the pendulum tiltmeter were reduced and a relatively low number of earthquakes occurred. The daily PSD was calculated by averaging the hourly PSD obtained using Welch's method (Welch 1967). To remove the impact of earthquakes in spectral shape, hourly traces whose maximum amplitude was within $1 \times 10^{-4} [m/s^2]$ were selected; this threshold was determined by manually checking the maximum amplitude of microseisms over a few months of tilt records. Approximately 600 traces were available from the 720 traces, and the ensemble PSD was calculated using Welch's method for each trace.

Figure 6 shows the ensemble PSDs of the tiltmeters and seismometers in the most noisy and quiet days in November 2022. The noisy and quiet day were selected by calculating the average of root mean square amplitude of timeseries acceleration for the two tiltmeters and four seismometers. November 17 and 28 were selected as the quiet and noisy days, respectively. A peak of microseism, which was between 0.1 and 5 Hz (Webb 1998), was observed in six PSDs. Between 0.1 and 1 Hz, the six PSDs showed almost the same shape. This confirms the validity of the observations in the seismic band. At values higher than 1 Hz, although the six PSDs varied
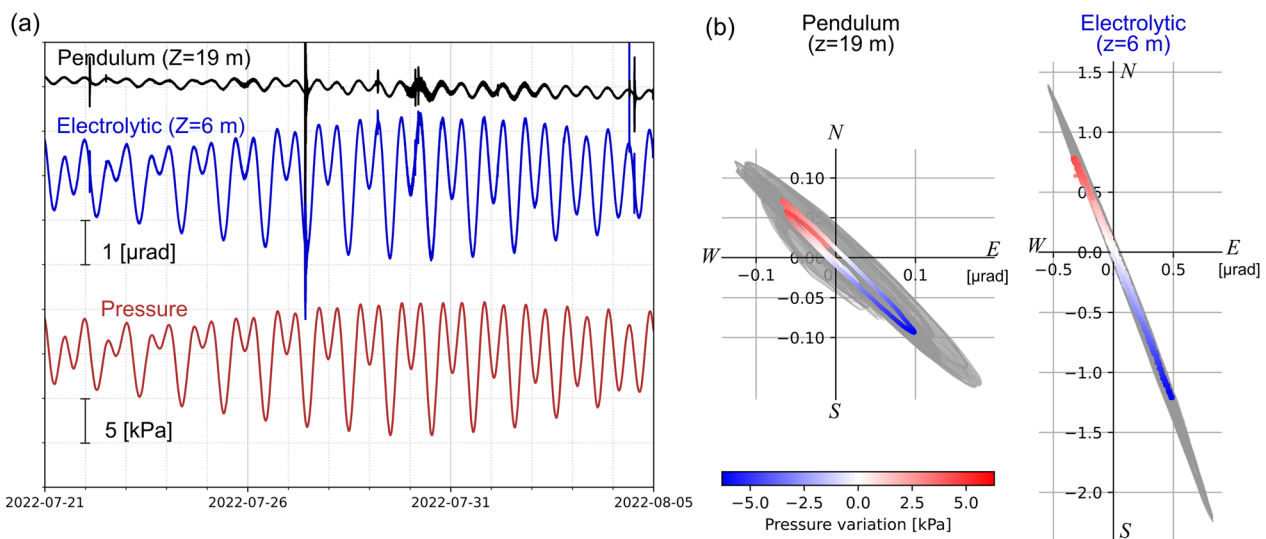

Fig. 5 Tidal responses of the two tiltmeters in one month. **a** Time series data of tilt and pressure. The direction with the largest amplitude of tidal response is shown for tilt variation. The pressure was measured at the nearest DONET station (KMB06, approximately 4 km from the tiltmeter). **b** Particle motion of the tilt recorded on July 5, 2022. The particle motion is colored according to the pressure variation. Positive values of tilt imply uplift in East and North directions for the horizontal and vertical directions, respectively. Gray lines are daily particle motions on days in July 2022 on which no significant earthquakes were recorded
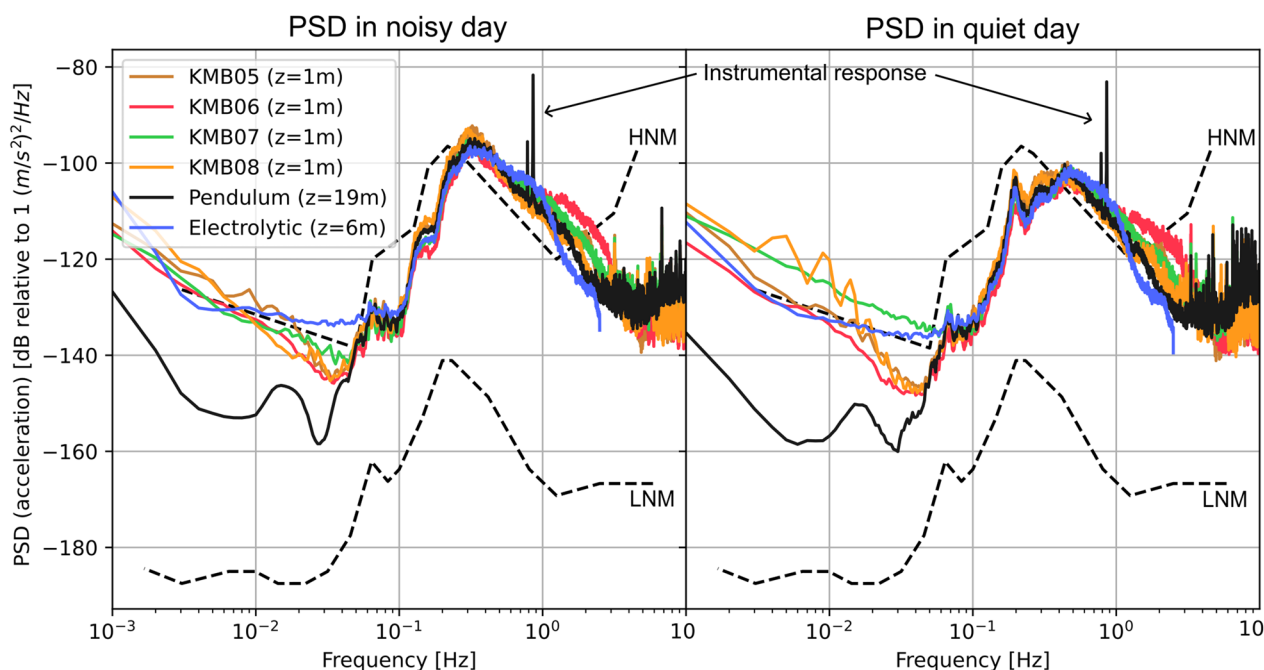
Tsuji *et al. Earth, Planets and Space* (2023) 75:188

Page 8 of 14

Fig. 6 Ensemble power spectrum density (PSD) of the two tiltmeters and four broadband seismometers around the tiltmeters (approximately 5—15 km away). The PSDs were calculated by averaging the ensemble power spectra of the hourly tilt records on the most noisy (left) and quiet (right) days in November 2022. The tilt records from the electrolytic tiltmeters were converted into acceleration records. Spikes around 0.8 Hz in the PSD of the pendulum tiltmeter are instrumental responses that remained after response calibration. Dashed lines with HNM and LNM are indicates the New High Noise and Low Noise models (Peterson 1993), respectively

largely, the variance was almost same as that among the four DONET stations around the tiltmeters. Below 0.02 Hz, the pendulum tiltmeter showed considerably lower power, which was up to 100 times lower relative to the others. This demonstrated the advantages of the pendulum tiltmeter as compared to that of the other sensors. The sensor depth (19 m below the seafloor) was approximately three times deeper than that of the electrolytic tiltmeter (6 m) and 20 times deeper than that of the seismometers at DONET stations (1 m). Between 0.01 and 0.05 Hz, the electrolytic tiltmeter exhibited a larger value, indicating the resolution limit of the instrument. The power in the frequency band was less than $10^{-3}[\mu rad^2/Hz]$ and is approximately 6 nrad in the time domain. This is almost the same level as the specification of 5 nrad for an electrolytic tiltmeter. Thus, the electrolytic tiltmeter could not show the advantage of a deeper location than DONET stations. At approximately 0.8 Hz, spikes were observed in the PSD of the pendulum tiltmeter, which were remaining instrumental responses after the response calibration process using Eq. (1). The spikes were observed around the natural frequencies of the pendulum of 0.78 Hz and 0.86 Hz which are those of test in the laboratory. We note that the lower PSD of the pendulum tiltmeter did not indicate lower sensitivity. Zumberge et al. (2018) performed a similar comparison with

an identical instrument except that it included a separate, vertical component to seismometers in a 60-m-deep borehole deployed in New Mexico, United States. The PSD of their observation also reached just below -180 dB relative to 1 $[(m/s^2)^2/Hz]$ in the horizontal components. In addition, only the pendulum tiltmeter observed an infragravity wave peak between 0.01 and 0.8 Hz. This also highlights the high detection capabilities of the pendulum tiltmeter and lower noise level in the deepest borehole.

The ensemble PSDs in Fig. 6 show the potential of the observations for VLFE detection because they show that the pendulum tiltmeter has a signal-to-noise ratio equal to or greater than that of the DONET stations. The DONET stations have sufficient signal-to-noise ratios to contribute to studies on VLEF (e.g., Yamamoto et al. 2022). Thus, the pendulum tiltmeter can contribute to this type of study. Furthermore, the amplitude of signals used in the Yamamoto et al. (2022) was in the order of hundreds of nano m/s at 0.02–0.05 Hz. In the area around the tiltmeters, no significant activities with VLFEs were detected by our observation network including DONET, in the period in which both tiltmeters have been in operation. If an event with the same signal amplitude as that reported by Yamamoto et al. (2022) occurred, the pendulum tiltmeter might be able to observe smaller

Tsuji *et al. Earth, Planets and Space*   (2023) 75:188

Page 9 of 14

events by taking advantage of the lower noise level. Contrary, the signal amplitude might be on the margins of the electrolytic tiltmeter. Since root-mean-square velocity of 100 nm/s at 0.03 Hz corresponds to − 130 dB in PSD of acceleration, a limited number of events might be observed relative to the other sensors.

In-situ estimation of sensitivity

A load experiment was conducted around the borehole to confirm a basic and important assumption that tiltmeters correctly measure the seafloor tilt. If the tiltmeters measure the ground tilt and the ground response follows an elastic medium, the results of the load experiment can be explained using the theoretical response of a half-space elastic medium.

The theoretical response was calculated using Boussinesq's solution, following Shimizu et al. (2007). This yields a theoretical response of the tilt by a point load on a half-space elastic medium. Equation (1) in Shimizu et al. (2007) provides the theoretical tilt at point of (x, y, z) due to a point load at $(x, y, z) = (0, 0, 0)$ as follows:

$$\phi_{tx} = \frac{(1+\nu)Px}{\pi E} \left\{ \frac{1-\nu}{\left(\sqrt{x^2+y^2+z^2}\right)^3} - \frac{3z^2}{2\left(\sqrt{x^2+y^2+z^2}\right)^5} \right\} \tag{2a}$$

$$\phi_{ty} = \frac{(1+\nu)Py}{\pi E} \left\{ \frac{1-\nu}{\left(\sqrt{x^2+y^2+z^2}\right)^3} - \frac{3z^2}{2\left(\sqrt{x^2+y^2+z^2}\right)^5} \right\} \tag{2b}$$

where ϕ_{tx} and ϕ_{ty} are the tilt responses in the X- and Y-directions, respectively. E and ν are Young's modulus and Poisson's ratio, respectively. P is the stress due to the point load.

In the experiment, a mass of 120 kg was placed on the seafloor around the heads of the boreholes using a remotely operated vehicle (ROV). The mass was placed in the X and Y axis of the tiltmeter sensor at the most sensitive distance, which was theoretically estimated based on Boussinesq's solution. The calculated distances were 2.5 and 8 m from the borehole head for the electrolytic and pendulum tiltmeters, respectively. This experiment was performed by ROV "Hyper Dolphine" on September 25, 2022, on the KS22-J06 cruise of the R/V Shinsei-maru. The response of the mass was measured using the following sequence. First, the ROV touched down on the seafloor and deployed the mass of 120 kg (gray period before the red period in each panel in the Fig. 7a). Then, the ROV lifted off from the seafloor without the mass (red periods in the Fig. 7a). After approximately 10 min, the ROV touched down on the seafloor again and collected the mass (gray period after the red period in each panel in the Fig. 7a).

The results of the load experiment are shown in Fig. 7a and Table 1. Figure 7a shows the tilt variation in the load experiment. A lowpass filter below 100 s was applied to enhance the signal of the experiment, however, to show the recovery of the response due to the mass, detrending was not applied to the tilt variation. Instead of the detrending, a lowpass filter below 6 h are used to reduce trend. Those are plotted in black and blue dashed lines for the pendulum and electrolytic tiltmeters, respectively.

Table 1 shows the measured change in tilt due to a load of 120 kg. The changes in tilt are estimated by searching an offset between tilt variations with the lowpass filters below 6 h and with that below 100 s in the red period in Fig. 7a. The best-fit values of the offsets are searched with intervals of 0.1 and 10 nano radians for the pendulum and electrolytic tiltmeters, respectively. Red dashed lines in Fig. 7a show the best-fit offsets. In the experiment, only the loading component showed a marked tilt response, whereas the other components showed none.

Elastic moduli were estimated to confirm that the results could be explained using a set of realistic parameters. For ease of comparison, Young's modulus and Poisson's ratio were characterized by density and by p- and s-seismic velocity, V_P and V_S, when calculating Boussinesq's solution. Additionally, because the weight was placed only in the X and Y directions of the sensor, one direction could be considered. Among the three elastic parameters, the V_S was the most effective. Thus, V_S was estimated by assuming a density and V_P of 1300 kg/m^3 and 1600 m/s, respectively. These values are representative of seafloor sediments. Consequently, the estimated V_S values are listed in Table 2.

The V_S values in Table 2 are within realistic ranges for seafloor sediments (Hamilton 1976). The results of the experiment and the theoretical response of a 120 kg point load at the most sensitive distance were plotted with several values for V_S in Fig. 7b. Considering the depths of the tiltmeters (6 and 19 m for the electrolytic and pendulum tiltmeters, respectively), V_S values of approximately 150 and 300 m/s were reasonable in the sedimentary layer. Additionally, it is consistent that the deeper sensor (pendulum tiltmeter) has a faster V_S than the shallower sensor (electrolytic tiltmeter).

Tidal responses

As previously mentioned, a large amplitude of tidal response was observed for both tiltmeters (Fig. 5). However, as shown in Fig. 5a, the amplitude of the tidal response differed between the two tiltmeters. Maximum amplitude of the tidal response for the electrolytic tiltmeter was up to 4 μrad and that for the pendulum tiltmeter was up to 0.4 μrad. The difference in root mean square amplitude was approximately 10 times between the two
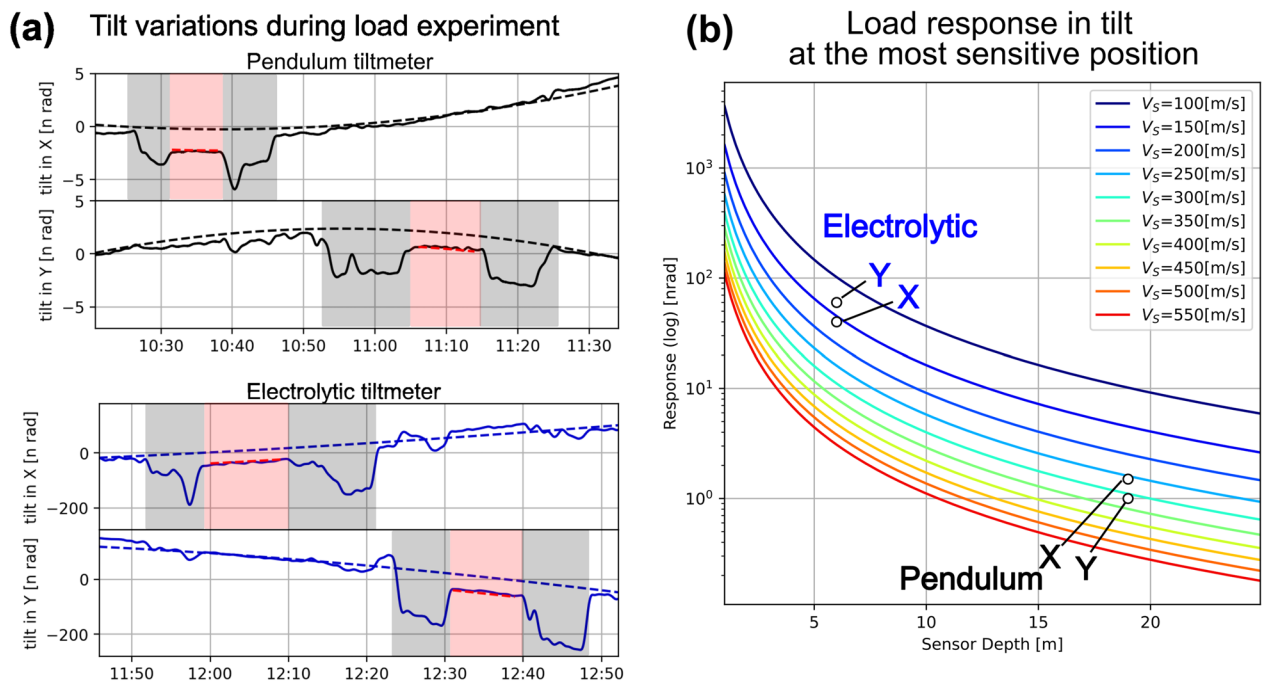
Tsuji *et al. Earth, Planets and Space*   (2023) 75:188

Page 10 of 14

Fig. 7 Results of the load experiments and their theoretical responses. **a** Tilt variations during the load experiment. Tilt variation in the X and Y direction of the sensor of the tiltmeter during the load experiment are shown for the pendulum (upper panel) and electrolytic (lower panel) tiltmeters. Gray and red shadows indicate periods when the ROV touched down and left the 120 kg of mass on the seafloor, respectively. Solid and dashed lines show tilt variations with low pass filter below 100 s and 6 h, respectively. Red dashed lines in the red periods show best-fit offsets (tilt changes of the load experiments shown in Table 1). **b** The theoretical load response for a half-space elastic medium at the most sensitive positions is shown with several elastic parameters (lines colored by V_S) and the results of the experiment (circles). The curves were calculated assuming a density and V_P of 1300 kg/m^3 and 1600 m/s, respectively

Table 1 Tilt changes of load experiment

	Electrolytic tiltmeter	Pendulum tiltmeter
X direction	40 [nrad]	1.5 [nrad]
Y direction	60 [nrad]	1.0 [nrad]

Table 2 V_S estimated by Boussinesq's solution with representative density and V_P

	Electrolytic tiltmeter	Pendulum tiltmeter
X direction	130 [m/s]	310 [m/s]
Y direction	160 [m/s]	260 [m/s]

tiltmeters. The amplitude of tidal response was equal or greater than the signal amplitude, which was in the order of 0.1 μrad of a slow slip event (SSE) calculated by Shinohara et al. (2003). Thus, the tidal responses had to be reduced to detect tilt variations by SSEs with better resolution. Because we aimed to develop a reduction method, we discuss possible mechanisms underlying the tidal responses.

To clarify the correlation with the tide, the pressure variation observed at the DONET station KMB06 was simultaneously plotted in Fig. 5a, which was located approximately 4 km in the SE direction. The tidal responses of both the tiltmeters correlated well with the M2 tide. The tilt variation in the direction of the maximum amplitude of the tidal response was plotted for each tiltmeter (Fig. 5a). The direction was estimated by fitting the tilt variation during each period of the M2 tide to an ellipse. The average direction of the major axis of the ellipse was used as the direction of the maximum amplitude of the tidal response. In the fitting, a band-pass filter between 13 and 11 h was applied to the tilt variations in July 2022 before dividing the tilt records into periods. The period used in the analysis was selected such that it did not include earthquake signals.

The relationship between tidal and pressure variations was analyzed. To visualize the relationship, the particle motions of the two tiltmeters were plotted on a representative day and colored with pressure variation, as shown in Fig. 5b. Since the period of the M2 tide was approximately 12 h, the particle motion during a day included two ellipses. The principal directions of the orbits of the particle motions for both tiltmeters were

Tsuji *et al. Earth, Planets and Space*   (2023) 75:188

Page 11 of 14

almost the same. The NW–SE direction was the sensitive direction of the tidal response. Additionally, the tendencies of the tilt with pressure perturbations were the same. High pressure corresponds to a downward tilt in the SE direction, while low pressure corresponds to an uplift tilt in the SE direction. The azimuthal dependencies were constant in the analyzed period. To show the variation, daily particle motions during days in July 2022 on which no significant earthquakes were recorded are shown as gray lines in Fig. 5b.

These characteristics on tidal response may reflect local structural characteristics. The observations showed that the tidal response in the tilt correlates well with the pressure change, suggesting that uniform loading and unloading caused by the movement of seawater resulted in a tidal response. However, in a uniformly elastic half-space medium, loading causes deformation only in the vertical direction. Thus, the tidal response indicates a difference in the elastic parameters in the horizontal direction, particularly in the sensitive direction.

The sensitive direction was almost the same as the downslope direction of the local bathymetry, especially for the electrolytic tiltmeter (Fig. 8a). The local bathymetry around the tiltmeter gently slopes downward in the SE direction, which could possibly be due to the difference in thickness of the soft sedimentary layer that caused a tidal response. If the thickness of the soft sedimentary layer increases in the downward direction of the slope, the magnitude of the deformation due to a unit of load or unload also increases. This can cause a difference in the vertical deformation along the slope and tilt variation even if the loading is uniform. Figure 8b shows a schematic diagram of this interpretation, explaining the

tendency of the tidal response to a downward tilt in the SE direction at high pressure and an uplift tilt in the NW direction at low pressure.

We performed a simple calculation to estimate the tilt response due to the difference in thickness of sedimentary layers using the elastic parameter estimated for the pendulum tiltmeter. We considered an elastic layer with the Young's modulus E that lays on a slope with an angle of θ (Additional file 1: Appendix 1). As a result, the tilt due to a stress P was $\frac{P\tan\theta}{E}$. The Young's modulus estimated by the load experiment of the pendulum tiltmeter and the electrolytic tiltmeter were $3.5 \times 10^8 Pa$ and $8.7 \times 10^7 Pa$, respectively. A representative change in pressure due to tide is 10^4 Pa. An acceptable tilt of slope is less than 5 degrees which was derived from the seismic cross-section created for IODP Site C0002 which has approximately the same geological structure (Moore et al 2014). The estimated tilts for slope angle of 1 degree with these values were 0.5 and 2.0 micro radians for the pendulum tiltmeter and electrolytic tiltmeter, respectively. These values are consistent with the observations in the order. However, the results of the calculation cannot explain the 10 times of difference in amplitude between the two tiltmeters. The estimated value for the electrolytic tiltmeter is $2 - 3$ times less than 4 micro radians of maximum amplitude in observation.

The larger response in the electrolytic tiltmeter is likely due to the other causes. A possibility is an effect of the casing of the borehole. In the load experiment, the mass was deployed at 2.5 m far from the borehole head. In this condition, the casing of the borehole also tilts with the surrounding media, thus, the relatively hard structure of the casing itself may cause a harder shear modulus.
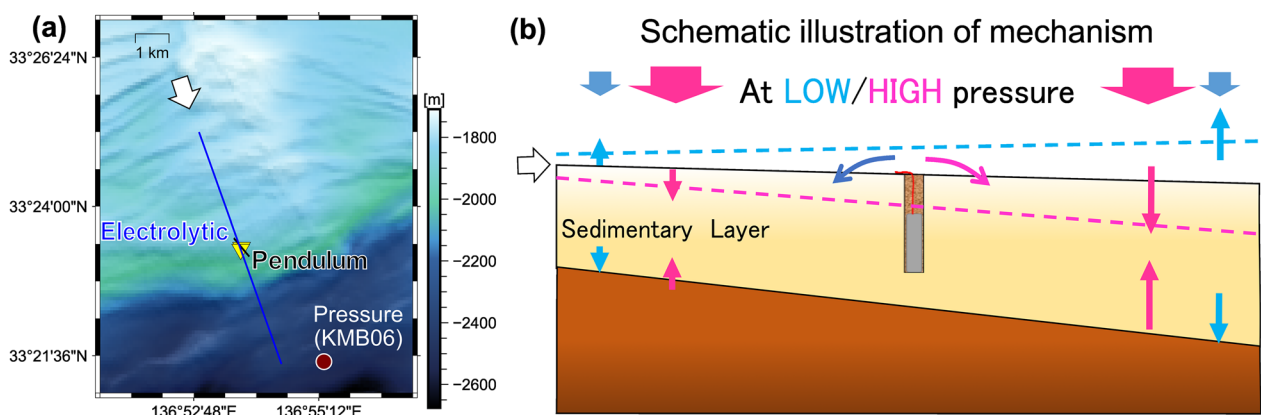

Fig. 8 **a** Sensitive directions and local bathymetry, and **b** a schematic image of the response to tidal pressure change. The black and blue lines in the map on the left indicate the sensitive directions of the tidal response at the electrolytic and pendulum tiltmeters, respectively. The white arrow with a black edge indicates the direction of a cross-section of the schematic image show in (**b**). The color of the arrows in **b** indicates the pressure conditions. Red and blue arrows indicate relatively high and low pressures, respectively. The red and blue dashed lines indicate the compression and expansion of the sedimentary layer under high- and low-pressure conditions, respectively

Tsuji *et al. Earth, Planets and Space*   (2023) 75:188

Page 12 of 14

In contrast, tidal pressure variation affects mainly vertical deformation. Thus, the effect of casing should be little. This difference might cause an underestimation of the tilt due to geological structure which we estimated before. Deformation of the pressure vessel due to hydrostatic pressure variations also makes a change in tilt, however, the magnitude estimated by a simulation was significantly smaller than the observation. The sensor of the electrolytic tiltmeter is mounted on a board, and the board is connected to the end-cap at the head of the cylindrical-shaped pressure vessel. However, the board is not connected across the center of the circles at the end-cap. In other words, the center of the board is offset relative to the center axis of the cylinder of pressure housing of the tiltmeter. Thus, the strength in the vertical direction is likely not uniform, which generates deformation differences in the pressure vessel due to variations in pressure. We estimated the magnitude of deformation for 10^4 Pa by a simulation with the finite element method. As a result, the effect of the deformation in tilt was less than 10^{-7} radians. Contrary, in the design of the pendulum tiltmeter, significant effort was aimed at minimizing the distortion to the physical structure from hydrostatic pressure that could otherwise produce an anomalous tilt. A finite element model was used to calculate the distortion to the structure from tidal variations. We concluded that the anomalous tilts in the tidal band caused by a distortion of the pressure vessel-tiltmeter frame combination will be less than 3 nano radians for the pendulum tiltmeter.

Conclusions

Two tiltmeters were installed in ocean bottom boreholes in the Kumano Basin along the Nankai Trough, Japan. An electrolytic tiltmeter was installed 6 m below the seafloor, while a second pendulum tiltmeter was developed for more precise observations and installed 19 m below the seafloor using a specific method with mortar.

Both tiltmeters continued precise measurements of ground tilt after 1–1.5 years of the initial drift. By analyzing the power spectral density, equal- or better-quality noise levels were confirmed in the seismic frequency ranges relative to a continuous seafloor seismic station in DONET. A large tilt variation correlating with the M2 tide (tidal response) was observed in both tiltmeters at different amplitudes. To reveal the mechanism of the tidal responses, the azimuthal dependence and its relationship with pressure variation were analyzed. As a result, a similar dependence was observed for both tiltmeters. The NW–SE direction was sensitive to the tidal response and uplift in the SE direction at low pressures. The sensitive direction was approximately the same as that of the slope of the local bathymetry. Amplitude

of tilt variations due to geological structure caused by tidal pressure variations was estimated with a simple model. The amplitude estimated for the pendulum tiltmeter was approximately the same as that of observation. However, the amplitude for the electrolytic tiltmeter was approximately two times smaller than that of observation. Furthermore, an in-situ load experiment with a mass of 120 kg was conducted to estimate an elastic parameter using a Boussinesq's solution, which confirmed that the surrounding medium of the tiltmeter can be considered an elastic body. Consequently, the response of the load experiment was explained using a set of realistic parameters.

Abbreviations

DONET   Dense Oceanfloor Network system for Earthquake and Tsunamis
LTBMS   Long-term borehole monitoring system
IODP   Integrated Ocean Drilling Program
VLFE   Very low frequency earthquake
SSE   Slow slip event
BMS   Boring Machine System
PSD   Power spectral density
ROV   Remotely operated vehicle
GPS   Global positioning system

Supplementary Information

The online version contains supplementary material available at https://doi.org/10.1186/s40623-023-01946-w.

> **Additional file1: Appendix 1.** Estimation of tilt due to difference in thickness of an elastic layer.

Author contributions
ST contributed to the analysis, load experiments, and manuscript writing. EA contributed to analysis and the project's management. TY and SN contributed to the installation of the instruments and the load experiment. YM contributed to the installation and management of the observational system used to acquire the data. MZ contributed to the development of the pendulum tiltmeter. KT contributed to the development of an installation method for the pendulum tiltmeters and instruments.

Availability of data and materials
The data observed by the DONET stations are available on the website of National Research Institute for Earth Science and Disaster Resilience (https://www.seafloor.bosai.go.jp/). Data observed using the borehole tiltmeters can be shared upon request with the corresponding authors.

Declarations

Ethics approval and consent to participate
Not applicable.

Author details
[1]Japan Agency for Marine-Earth Science and Technology (JAMSTEC), Natsu-shima-cho 2-15, Yokosuka, Kanagawa 237-0061, Japan. [2]University of California San Diego, Mail Code 0225, 9500 Gilman Drive, La Jolla, San Diego, CA 92093-0225, USA. [3]Research and Development Center, Mitsubishi UBE Cement Corporation, 1-6 Okinoyama Kogushi, Ube 755-8633, Japan.

References

Ando M (1975) Source mechanisms and tectonic significance of historical earthquakes along the Nankai Trough, Japan. Tectonophysics 27:119–140. https://doi.org/10.1016/0040-1951(75)90102-X

Annoura S, Hashimoto T, Kamaya N, Katsumata A (2017) Shallow episodic tremor near the Nankai Trough axis off southeast Mie Prefecture. Jpn Geophys Res Lett 44:3564–3571. https://doi.org/10.1002/2017GL073006

Araki E, Yokobiki T, Kawaguchi K, Kaneda Y (2013) Background seismic noise level in DONET seafloor cabled observation network. IEEE Int Underw Technol Symp (UT) 2013:1–4. https://doi.org/10.1109/UT.2013.6519858

Araki E, Saffer DM, Kopf AJ, Wallace LM, Kimura T, Machida Y, Ide S, Davis E, IODP Expedition 365 shipboard scientists (2017) Recurring and triggered slow-slip events near the trench at the Nankai Trough subduction megathrust. Science 356:1157–1160. https://doi.org/10.1126/science.aan3120

Argus DF, Gordon RG, DeMets C (2011) Geologically current motion of 56 plates relative to the no-net-rotation reference frame. Geochem Geophys Geosyst. https://doi.org/10.1029/2011GC003751

Ariyoshi K, Iinuma T, Nakano M, Kimura T, Araki E, Machida Y, Sueki K, Yada S, Nishiyama T, Suzuki K, Hori T, Takahashi N, Kodaira S (2021) Characteristics of slow slip event in March 2020 revealed from borehole and DONET observatories. Front Earth Sci 8:600793. https://doi.org/10.3389/feart.2020.600793

Beyreuther M, Barsch R, Krischer L, Megies T, Behr Y, Wassermann J (2010) ObsPy: a python toolbox for seismology. Seismol Res Lett 81:530–533. https://doi.org/10.1785/gssrl.81.3.530

Hamilton EL (1976) Shear-wave velocity versus depth in marine sediments: a review. Geophysics 41:985–996. https://doi.org/10.1190/1.1440676

Harris CR, Millman KJ, van der Walt SJ et al (2020) Array programming with NumPy. Nature 585:357–362. https://doi.org/10.1038/s41586-020-2649-2

Hunter JD (2007) Matplotlib: a 2D graphics environment. Comp Sci Eng 9:90–95. https://doi.org/10.1109/MCSE.2007.55

Japan Meteorological Agency (2004) The earthquake SE off Kii peninsula on September 5, in the summary of the 159 meeting of the Coordinating Committee for Earthquake Prediction, Japan, https://cais.gsi.go.jp/YOCHIREN/activity/159/159.html. Accessed 1 Dec 2023. (**In Japanese**)

Kaneda Y, Kawaguchi K, Araki E, Matsumoto H, Nakamura T, Kamiya S, Ariyoshi K, Hori T, Baba T, Takahashi N (2015) Development and application of an advanced ocean floor network system for megathrust earthquakes and tsunamis. In: Favali P, Beranzoli L, De Santis A (eds) Seafloor observatories. Springer, Heidelberg, pp 643–666

Kawaguchi K, Araki E, Kaneda Y (2011) Establishment of a method for real-time and long-term seafloor monitoring. J Adv Mar Sci Tech Soc 17:125–135. https://doi.org/10.14928/amstec.17.2_125

Kawaguchi K, Kaneko S, Nishida T, Komine T (2015) Construction of the DONET real-time seafloor observatory for earthquakes and tsunami monitoring. Seafloor observatories. Springer Praxis Books, Heidelberg, pp 211–228

Kido M, Fujimoto H, Miura S, Osada Y, Tsuka K, Tabei T (2006) Seafloor displacement at Kumano-nada caused by the 2004 off Kii Peninsula earthquakes, detected through repeated GPS/Acoustic surveys. Earth Planets Space 58:911–915. https://doi.org/10.1186/BF03351996

Kimura T, Araki E, Takayama H, Kitada K, Kinoshita M, Namba Y, Kyo M (2013) Development and performance tests of a sensor suite for a long-term borehole monitoring system in seafloor settings in the Nankai Trough, Japan. IEEE J Oceanic Eng 38:383–395. https://doi.org/10.1109/JOE.2012.2225293

Kimura T, Araki E, Yokobiki T, Nishida S, Matthew JC, Zumberge M, Takahashi K, Hori H, Kodaira S (2021) Real-time SSE monitoring by optical borehole tilt-meter in the Nankai Trough, Japan, Abstract of Japan Geoscience Union Meeting 2021, SCG51–05, May 30 – June 6, 2021, Online.

Moore GF, Kanagawa K, Strasser M, Dugan B, Maeda L, Toczko S, the IODP Expedition 338 Scientific Party (2014) IODP expedition 338: NanTroSEIZE stage 3: NanTroSEIZE plate boundary deep riser 2. Sci Dril 17:1–12. https://doi.org/10.5194/sd-17-1-2014

Nakano M, Tonegawa T, Kaneda Y (2012) Orientations of DONET seismometers estimated from seismic waveforms. JAMSTEC Rep Res Dev 15:77–89. https://doi.org/10.5918/jamstecr.15.77.(inJapanesewithEnglishabstract)

Nakano M, Hori T, Araki E, Kodaira S, Ide S (2018) Shallow very-low-frequency earthquakes accompany slow slip events in the Nankai subduction zone. Nat Commun 9:984. https://doi.org/10.1038/s41467-018-03431-5

National Research Institute for Earth Science and Disaster Resilience (2019). Nied DONET, National Research Institute for Earth Science and Disaster Resilience. https://doi.org/10.17598/NIED.0008

Nishimura T, Yokota Y, Tadokoro K, Ochi T (2018) Strain partitioning and inter-polate coupling along the northern margin of the Philippine Sea plate, estimated from Global Navigation Satellite System and Global Positioning System-Acoustic data. Geosphere 14:535–551. https://doi.org/10.1130/GES01529.1

Obana K, Kodaira S (2009) Low-frequency tremors associated with reverse faults in a shallow accretionary prism. Earth Planet Sci Lett 287:168–174. https://doi.org/10.1016/j.epsl.2009.08.005

Peterson J (1993) Observation and modeling of seismic background noise. USGS Technical Report 93–322, https://doi.org/10.3133/ofr93322.

Shimizu T, Onishi K, Matsuoka T, Fujita M, Takahashi M (2007) Estimation of the tilt variations influenced by snow-removal and rainfall -Application of load test and tank model-, journal of the Society of Materials Science Japan. J Soc Mater Sci 56:839–845. https://doi.org/10.2472/jsms.56.839(inJapanesewithEnglishabstract)

Shinohara M, Araki E, Kamata M, Kinoshita M, Kyo N, Kuroki K, Kosuge Y, Kobayashi S, Konno S, Goto T, Saito S, Suzuki M, Takahashi T, Tadokoro K, Tsunogai U, Tezuka K, Nanba K, Nishi M, Hino R, Mikada H, Morita N, Yoshida C, Ito H (2003) Long-Term Monitoring Using Deep Seafloor Boreholes Penetrating the Seismogenic Zone. Bull Earthq Res Inst Univ Tokyo 78(2):205–218. https://doi.org/10.15083/0000032564

Takahashi K, Kawabata Y, Iwanami M, Kobayashi M, Kasaya T, Yamanaka T, Nomura S, Makita H (2022) In-situ deep-sea monitoring of cement mortar specimen at a depth of 3515 m and changes in mechanical properties after exposure to deep sea condition. J Adv Concr Technol 20(3):254–266. https://doi.org/10.3151/jact.20.254

Takemura S, Obara K, Shiomi K, Baba S (2022) Spatiotemporal variations of shallow very low frequency earthquake activity southeast off the Kii Peninsula, along the Nankai Trough. Jpn J Geophys Res Solid Earth 127(JB023073):e2021. https://doi.org/10.1029/2021JB023073

Tamaribuchi K, Kobayashi A, Nishimiya T, Hirose F, Annoura S (2019) Characteristics of shallow low-frequency earthquakes off the Kii Peninsula, Japan, in 2004 revealed by ocean bottom seismometers. Geophys Res Let 46:13737–13745. https://doi.org/10.1029/2019GL085158

Toh A, Chen WJ, Takeuchi N, Dreger DS, Chi WC, Ide S (2020) Influence of a sub-ducted oceanic ridge on the distribution of shallow VLFEs in the Nankai Trough as revealed by moment tensor inversion and cluster analysis. Geophys Res Let 47(GL087244):e2020. https://doi.org/10.1029/2020GL087244

Urabe T, Tsukada S (1992) Win-A workstation program for processing wave-form data from microearthquake networks. Abstr Seismol Soc Jpn 2:41 (**in Japanese**)

Virtanen P, Gommers R, Oliphant TE, Haberland M, Reddy T, Cournapeau D, Burovski E, Peterson P, Weckesser W, Bright J, Van der Walt SJ (2020) SciPy 10: Fundamental algorithms for scientific computing in python. Nat Methods 17:261–272. https://doi.org/10.1038/s41592-019-0686-2

Webb SC (1998) Broadband seismology and noise under the ocean. Rev Geop 36:105–142. https://doi.org/10.1029/97RG02287

Welch P (1967) The use of the fast Fourier transform for the estimation of power spectra: A method based on time averaging over short, modified

periodograms. IEEE Trans Audio Electroacoust 15(2):70–73. https://doi.org/10.1109/TAU.1967.1161901

Wessel P, Luis JF, Uieda L, Scharroo R, Wobbe F, Smith WHF, Tian D (2019) The Generic Mapping Tools version 6. Geochem Geophys Geosyst 20:5556–5564. https://doi.org/10.1029/2019GC008515

Yamamoto Y, Ariyoshi K, Yada S, Nakano M, Hori T (2022) Spatio-temporal distribution of shallow very-low-frequency earthquakes between December 2020 and January 2021 in Kumano-nada, Nankai subduction zone, detected by a permanent seafloor seismic network. Earth Planets Space 74:14. https://doi.org/10.1186/s40623-022-01573-x

Yokibiki T, Nishida S, Kimura T, Tusji S, Murashima T, Takase K, Takahashi K, Araki E (2023) Construction of the borehole observatory site using Boring Machine System. Int Symp Underw Tech 2023. UT

Yokota Y, Ishikawa T, Watanabe S, Tashiro T, Asada A (2016) Seafloor geodetic constraints on interplate coupling of the Nankai Trough megathrust zone. Nature 534:374–377. https://doi.org/10.1038/nature17632

Zumberge MA, Berger J, Dzieciuch MA, Parker RL (2004) Resolving quadrature fringes in real time. Appl Opt 43:771–775. https://doi.org/10.1364/AO.43.000771

Zumberge M, Berger J, Hatfield W, Wielandt E (2018) A three-component borehole optical seismic and geodetic sensor. Bull Seismol Soc Am 108:2022–2031. https://doi.org/10.1785/0120180045

Publisher's Note